

# Deep transfer learning for partial differential equations under conditional shift with DeepONet

Somdatta Goswami<sup>a,1</sup>, Katiana Kontolati<sup>b,1</sup>, Michael D. Shields<sup>b</sup>, George Em Karniadakis<sup>a,c,\*</sup>

<sup>a</sup>*Division of Applied Mathematics, Brown University*

<sup>b</sup>*Department of Civil and Systems Engineering, Johns Hopkins University*

<sup>c</sup>*School of Engineering, Brown University*

---

## Abstract

Traditional machine learning algorithms are designed to learn in isolation, i.e. address single tasks. The core idea of transfer learning (TL) is that knowledge gained in learning to perform one task (source) can be leveraged to improve learning performance in a related, but different, task (target). TL leverages and transfers previously acquired knowledge to address the expense of data acquisition and labeling, potential computational power limitations, and the dataset distribution mismatches. Although significant progress has been made in the fields of image processing, speech recognition, and natural language processing (for classification and regression) for TL, little work has been done in the field of scientific machine learning for functional regression and uncertainty quantification in partial differential equations. In this work, we propose a novel TL framework for task-specific learning under conditional shift with a deep operator network (DeepONet). Inspired by the conditional embedding operator theory, we measure the statistical distance between the source domain and the target feature domain by embedding conditional distributions onto a reproducing kernel Hilbert space. Task-specific operator learning is accomplished by fine-tuning task-specific layers of the target DeepONet using a hybrid loss function that allows for the matching of individual target samples while also preserving the global properties of the conditional distribution of target data. We demonstrate the advantages of our approach for various TL scenarios involving nonlinear PDEs under conditional shift. Our results include geometry domain adaptation and show that the proposed TL framework enables fast and efficient multi-task operator learning, despite significant differences between the source and target domains.

*Keywords:* transfer learning, domain adaptation, DeepONet, conditional shift, scientific machine learning, neural operators

---

\*Corresponding author.

Email addresses: [somdatta\\_goswami@brown.edu](mailto:somdatta_goswami@brown.edu) (Somdatta Goswami), [kontolati@jhu.edu](mailto:kontolati@jhu.edu) (Katiana Kontolati), [michael.shields@jhu.edu](mailto:michael.shields@jhu.edu) (Michael D. Shields), [george\\_karniadakis@brown.edu](mailto:george_karniadakis@brown.edu) (George Em Karniadakis)

<sup>1</sup>These authors contributed equally to this work.

## 1. Introduction

Deep learning has been successfully employed to replace expensive numerical solvers of complex physical processes and achieve unprecedented performance that allows the acceleration of numerous tasks including uncertainty quantification (UQ), risk modeling and design optimization [1–6]. Despite this success, often the predictive performance of such models is limited by the availability of labeled data used for training. However, in many cases collecting large and sufficient labeled datasets can be computationally intractable (e.g., when high-fidelity or multi-scale models are considered). Furthermore, learning in isolation, i.e. training a single predictive model for different but related single tasks, can be extremely expensive. To tackle this bottleneck, knowledge between relevant domains can be leveraged in a framework known as *transfer learning* (TL) [7]. In this scenario, information from a model trained on a specific domain (*source*) with sufficient labeled data can be transferred to a different but closely relevant domain (*target*) for which only a small number of training data is available.

In machine learning, TL is a popular and promising area and has been applied to address the issue of data scarcity in various problems, including image recognition [8, 9] and natural language processing (NLP) [10, 11]. The most important prerequisite in TL is that there needs to be a connection between the learning domains. In fact, one proposed categorization of TL approaches is based on the consistency between the distributions of source and the target input (or feature) spaces and output (or label) spaces [12]. The shift between the source and target data distributions is considered the major challenge in modern TL. Types of distribution shifts include conditional shift, where the marginal distribution of source and target input data remains the same while the conditional distributions of the outputs differs (i.e.  $P(\mathbf{x}_s) = P(\mathbf{x}_t)$  and  $P(\mathbf{y}_s|\mathbf{x}_s) \neq P(\mathbf{y}_t|\mathbf{x}_t)$ ) and covariate shift where the opposite occurs (i.e.  $P(\mathbf{x}_s) \neq P(\mathbf{x}_t)$  and  $P(\mathbf{y}_s|\mathbf{x}_s) = P(\mathbf{y}_t|\mathbf{x}_t)$ ). TL for problems under covariate shift have been explored primarily for classification and more recently for regression tasks [13, 14]. State-of-the-art approaches for regression problems under conditional shift include the Transfer Learning by Boosting (TLB) [15], the Residual Approximation (RA) [16], General Transformation Function (GTF) [17] and Domain Adaptation Under GeTarS [18] and more recently ResTL, an approach based on fuzzy residuals [19], and RSD+BMP based on a representation subspace distance and bases mismatch penalization [20]. Zhang and Garikipati proposed [21] Knowledge-Based Neural Networks (KBNNs) which leverage dominant characteristics of the data to study evolving microstructures. Recently, approaches based on Physics-Informed Neural Networks (PINNs) [22–25], have been proposed to solve PDE problems under distribution shift.

Motivated by the lack of TL approaches for task-specific operator learning and UQ, in this work we present a novel framework for efficient TL under conditional shift using neural operators. The main idea behind this work is to train a source model with sufficient labeled data (i.e., model evaluations) from a source domain under a standard regression loss and transfer the learned variables to a second target model, which is trained with very limited labeled data from a target domain under a hybrid loss function. The hybrid loss is comprised of a regression loss and the conditional embedding operator discrepancy (CEOD) loss [20], used to measure the difference between conditional distributions in a reproducing kernel Hilbert space (RKHS). The key ingredient of the proposed framework is the exploitation of domain-

invariant features extracted by the source model, which leads to the efficient initialization of the target model variables. It is widely accepted that lower layers are in charge of more general features [26], thus fine-tuning of the target model focuses on training higher levels of the network. As a surrogate model we employ the recently proposed deep neural operator or DeepONet [4]. While most surrogate modeling techniques, such as standard neural networks, aim to simply approximate a mapping representing the solution of a PDE on fixed discretized domains, DeepONet is discretization-invariant and allows us to fully learn the operator and thus perform real-time prediction for arbitrary new inputs and domains. Importantly, the proposed framework, enables the identification of the PDE operator in domains, where very limited labeled data are available. To the best of our knowledge this is the first comprehensive study on the implementation of TL for operator learning in PDE problems. The main contributions of this work can be summarized in the following points:

- We propose a novel framework for transfer learning problems under conditional shift with deep neural operators.
- The proposed framework can be employed for fast and efficient task-specific PDE learning and uncertainty quantification.
- We leverage principles of the reproducing kernel Hilbert space (RKHS) and the conditional embedding operator theory to construct a hybrid loss function and finetune the target model.
- The computational advantages of the proposed framework are demonstrated through a variety of transfer learning problems, including geometry domain adaptation and involving nonlinear PDEs under various distribution shift scenarios.

The paper is organized as follows. In Section 2, we describe the transfer learning scenario and the basics of the DeepONet model for surrogate modeling. In Section 3, we present in detail the proposed methodology for transfer learning under conditional shift in PDE problems. In Section 4, we present experimental results for four transfer learning applications. Finally, we summarize our observations and provide concluding remarks in Section 5.

## 2. Preliminaries

### 2.1. Transfer learning scenarios

Consider a nonlinear and high-fidelity PDE model describing a physical process and a corresponding (usually expensive) numerical simulator (e.g., a finite-difference or finite-element solver). In a standard UQ setting, we aim to approximate the mapping  $f(\mathbf{x})$ , between a vector of input random variables,  $\mathbf{x}_i \in \mathcal{X}$ , and corresponding output quantities of interest (QoIs),  $f(\mathbf{x}_i) = \mathbf{y}_i \in \mathcal{Y}$ . We denote the input realizations (or instances) as  $\mathbf{X} = \{\mathbf{x}_1, \dots, \mathbf{x}_N\}$  and the associated QoIs as  $\mathbf{Y} = \{\mathbf{y}_1, \dots, \mathbf{y}_N\}$ . Thus, model  $f$  performs the mapping  $f : \mathbf{x}_i \in \mathbb{R}^{D_{\text{in}}} \rightarrow \mathbf{y}_i \in \mathbb{R}^{D_{\text{out}}}$  where the dimensionality of both the inputs and the outputs,  $D_{\text{in}}, D_{\text{out}}$  is usually high, e.g.,  $\mathcal{O}(10^{2-4})$ . Here, the high-dimensional inputs may represent random fields and/or processes, such as spatially or temporally varying coefficients, and the corresponding QoIs represent physical quantities, which can also vary in both space

and time. In this regression setting, we aim to approximate the mapping,  $f$ , based on a training dataset of  $N$  input-output pairs,  $(\mathbf{X} = \{\mathbf{x}_1, \dots, \mathbf{x}_N\}, \mathbf{Y} = \{\mathbf{y}_1, \dots, \mathbf{y}_N\})$ , and achieve the lowest possible predictive error.

Suppose that a surrogate  $f_s$ , is learned on a **source domain**, i.e., under specified conditions based on a dataset with  $N_s$  sufficient labeled data is generated  $\mathcal{D}_s = \{(\mathbf{x}_i^s, \mathbf{y}_i^s)\}_{i=1}^{N_s}$ . The generated dataset is composed of two parts: the random input realizations  $\mathbf{x}_i^s \in \mathcal{X}_s$  and the corresponding labels  $\mathbf{y}_i^s \in \mathcal{Y}_s$ . Consider now a second **target domain** corresponding to different problem conditions. These conditions might represent the simulation box geometry, boundary conditions, model parameters etc. Let us assume that only few available labeled target data exist in  $\mathcal{D}_t = \{(\mathbf{x}_i^t, \mathbf{y}_i^t)\}_{i=1}^{N_t}$ , where  $\mathbf{x}_i^t \in \mathcal{X}_T$ ,  $\mathbf{y}_i^t \in \mathcal{Y}_T$  and  $N_t \ll N_s$ . In addition, we assume that there exists a covariate shift, under which the marginal distribution (inputs) remains the same  $P(\mathbf{x}_s) = P(\mathbf{x}_t)$ , while the conditional distributions (QoIs) are different  $P(\mathbf{y}_s|\mathbf{x}_s) \neq P(\mathbf{y}_t|\mathbf{x}_t)$ . In cases where multiple target tasks exist, collecting sufficient labeled data can be computationally prohibitive. Furthermore, training a surrogate for target tasks with scarce data can lead to overfitting. Therefore, in this work we aim to construct fast and efficient surrogates  $f_t$  for target tasks by leveraging and transferring information between different but related domains,  $\mathcal{D}_s$  and  $\mathcal{D}_t$ , without the need of re-training models from scratch with random initialization. As a surrogate model we will employ the deep neural operator or DeepONet [4], a neural network-based method, which enables task-specific learning of PDE operators. More information on the DeepONet is given in the next Section.

## 2.2. Deep operator network (DeepONet)

Deep neural networks (DNNs) have been demonstrated to be an effective and versatile tool for problems where the solutions are ambiguous or there is insufficient knowledge about the relationships between the inputs and the outputs. The ability of DNNs to approximate arbitrary continuous functions on compact domains is a key advantage. Training DNNs, on the other hand, is done for differential equations with fixed inputs, such as initial conditions, boundary conditions, forcing, and coefficients. If one of the inputs is changed, the training process must be restarted. It is difficult to obtain real-time outputs for multiphysics systems that require multiple sets.

Operator learning, which is inspired by the universal approximation theorem, can be used to overcome the limitation of functional regression. DeepONet's seminal work on learning diverse continuous nonlinear operators motivated our work. DeepONet is particularly influenced by theory that guarantees small approximation error (that is, the error between the target operator and the class of neural networks of a given finite-size architecture). Before delving into the solution operators of the parametric PDEs, it is critical to understand the distinction between function regression and operator regression. The solution operator in the function regression approach is parametrized as a neural network between finite dimensional Euclidean spaces:  $C : \mathbb{R}^{d_1} \rightarrow \mathbb{R}^{d_1}$ , where  $d_1$  is the number of discretization points. In operator regression, however, a function is mapped to another function using an operator. In other words, it is the transformation of one infinite-dimensional space into another infinite-dimensional space. By learning the non-linear operator from the data, the operators would be trained to approximate the solution of the input functions using operator regression.

The DeepONet architecture consists of two DNNs: the branch net encodes the input function,  $\mathbf{X}$ , at fixed sensor points,  $\{x_1, x_2, \dots, x_m\}$ , while the trunk net encodes the information

related to the spatio-temporal coordinates,  $\zeta = \{x_i, y_i, t_i\}$ , at which the solution operator is evaluated to compute the loss function. When a physical system is described by PDEs, it involves multiple function, e.g., the PDE solution,  $\mathbf{u}(x, t)$ , the forcing term,  $\mathbf{f}(x, t)$ , the initial condition,  $\mathbf{u}_0(x)$ , and the boundary conditions,  $\mathbf{u}_b(x, t)$ , where  $x$  and  $t$  are the spatial and the temporal coordinates, respectively. We are usually interested in one of these functions, which is the output of the solution operator, and try to predict it based on the varied forms of the other functions, which is the input to the branch net. The trunk net takes as input the spatial and the temporal coordinates, e.g.  $\zeta = \{x_i, y_i, t_i\}$ , at which the solution operator is evaluated to compute the loss function.

Consider a computational model,  $\mathcal{M}(\mathbf{x})$ , where  $\mathbf{x}_i = \{\mathbf{x}_i(x_1), \mathbf{x}_i(x_2), \dots, \mathbf{x}_i(x_m)\}$  (point-wise evaluation of the input function to the branch net), which simulates a physical process and represents a mapping between a vector of input random variables,  $\mathbf{x}(\zeta) \in \mathbb{R}^{D_{\text{in}}}$ , and corresponding output quantities of interest (QoIs),  $\mathbf{y}(\zeta) \in \mathbb{R}^{D_{\text{out}}}$  where  $\zeta$  represent spatio-temporal coordinates. The goal of the DeepONet is to learn the solution operator,  $\mathcal{G}(\mathbf{x})$  that approximates  $\mathcal{M}(\mathbf{x})$ , and can be evaluated at continuous spatio-temporal coordinates,  $\zeta$  (input to the trunk net). The output of the DeepONet for a specified input vector,  $\mathbf{x}_i$ , is a scalar-valued function of  $\zeta$  expressed as  $\mathcal{G}_{\boldsymbol{\theta}}(\mathbf{x}_i)(\zeta)$ , where  $\boldsymbol{\theta} = (\mathbf{W}, \mathbf{b})$  includes the trainable parameters (weights,  $\mathbf{W}$ , and biases,  $\mathbf{b}$ ) of the networks.

The solution operator for an input realization,  $\mathbf{x}_1$ , can be expressed as:

$$\mathcal{G}_{\boldsymbol{\theta}}(\mathbf{x}_1)(\zeta) = \sum_{i=1}^p b_i \cdot tr_i = \sum_{i=1}^p b_i(\mathbf{x}_1(x_1), \mathbf{x}_1(x_2), \dots, \mathbf{x}_1(x_m)) \cdot tr_i(\zeta), \quad (1)$$

where  $b_1, b_2, \dots, b_p$  are outputs of the branch net and  $tr_1, tr_2, \dots, tr_p$  are outputs of the trunk net. Conventionally, the trainable parameters of the DeepONet, represented by  $\boldsymbol{\theta}$  in Eq. (1), are obtained by minimizing a loss function, which is expressed as:

$$\mathcal{L}(\boldsymbol{\theta}) = \mathcal{L}_r(\boldsymbol{\theta}) + \mathcal{L}_i(\boldsymbol{\theta}), \quad (2)$$

where  $\mathcal{L}_r(\boldsymbol{\theta})$  and  $\mathcal{L}_i(\boldsymbol{\theta})$  denote the residual loss and the initial condition loss, respectively.

The DeepONet model provides a flexible paradigm that does not limit the branch and trunk networks to any particular architecture. For an equispaced discretization of the input function, a convolutional neural network (CNN) could be used for the branch net architecture, while for a sparse representation of the input function, one could also use a feedforward neural network (FNN). A standard practice is to use a FNN for the trunk network to take advantage of the low dimensions of the evaluation points,  $\zeta$ .

Although the original DeepONet architecture proposed in [4] has shown remarkable success, several extensions have been proposed in [27] and [28] to modify its implementation and produce efficient and robust architectures. For instance, in the POD-DeepONet the basis functions for the trunk net are computed by performing proper orthogonal decomposition (POD) on the training data and using these basis in place of the trunk net. Additionally, the self-adaptive weights in the loss function of the DeepONet helps to automatically maneuver for the optimal penalizing parameter for different terms in the loss function to approximate systems with steep gradients.

### 3. Methodology

#### 3.1. Problem setup

Consider a multi-dimensional function  $f(\mathbf{x})$ , which represents the mapping between a vector of input random variables,  $\mathbf{x}_i \in \mathcal{X}$ , and the corresponding output QoIs,  $\mathbf{y}_i \in \mathcal{Y}$ . Furthermore, consider a source domain for which  $N_s$  sufficient labeled data have been generated  $\mathcal{D}_s = \{(\mathbf{x}_i^s, \mathbf{y}_i^s)\}_{i=1}^{N_s}$ , where  $\mathbf{x}_i^s \in \mathcal{X}_s$  and  $\mathbf{y}_i^s \in \mathcal{Y}_s$ . In addition, there exists a target domain with very few  $N_t$  available labeled data, and a set of  $N_u$  additional unlabeled data, i.e.,  $\mathcal{D}_t = \{(\mathbf{x}_i^{tL}, \mathbf{y}_i^{tL})\}_{i=1}^{N_t} \cup \{\mathbf{x}_j^{tU}\}_{j=1}^{N_u}$ , where  $\mathbf{x}_i^{tL}, \mathbf{x}_j^{tU} \in \mathcal{X}_s$  and  $\mathbf{y}_i^{tL} \in \mathcal{Y}_T$ . Thus, we focus on transfer learning under conditional shift, where the marginal distributions are identical ( $\mathcal{X}_s$ ) and the conditional distributions differ ( $\mathcal{Y}_s \neq \mathcal{Y}_T$ ).

#### 3.2. Measuring the distribution discrepancy

An important task in TL is to accurately compute the discrepancy between conditional distributions. While domain adaptation problems focus on minimizing the discrepancy between source and target distributions, here we aim to address the distribution shift between the labeled target data  $\{\mathbf{y}_i^{tL}\}_{i=1}^{N_t}$  and the surrogate prediction on the unlabeled target data  $\{f_T(\mathbf{x}_i^{tU})\}_{i=1}^{N_u}$ . Several approaches have been proposed for measuring the discrepancy or *divergence* between the marginal and conditional distributions. Early methods relied on the estimation of the underlying distributions via density estimation methods, such as kernel density estimation (KDE) [29]. However, when real-world high-dimensional data are considered, density estimation can be very challenging, and thus modern approaches avoid this intermediate step altogether. Yu et al. [30], proposed a new statistic which operates on the cone of symmetric positive semidefinite (SPS) matrix using the Bregman matrix divergence and used the cross entropy function to explicitly incorporate higher order information in the data. An alternative approach is to compute the distance metric through the embedding of probability measures in a reproducing kernel Hilbert space (RKHS). A RKHS  $\mathcal{H}$ , is a Hilbert space where all evaluation functionals in  $\mathcal{H}$  are bounded [31]. In such methods, the difference between the mean embedding in RKHS is computed like in Maximum Mean Discrepancy (MMD) proposed by Gretton et al. [32], which operates on marginal distributions. In this work, we employ a measure developed for conditional distributions, and thus below we briefly present some necessary preliminaries of the conditional embedding operator (CEO) theory.

##### 3.2.1. Conditional embedding operator theory

Consider two random variables  $X$  and  $Y$ , with  $\Omega_X, \Omega_Y$  and  $\mathcal{H}, \mathcal{F}$  being the original and RKHS spaces respectively. The conditional mean embedding of  $P(Y|X)$  can be defined as [33]:

$$\mu_{Y|X} := \mathbb{E}_{Y|X}[\psi(Y)|X = \mathbf{x}] = \mathcal{C}_{Y|X}\phi(\mathbf{x}), \quad (3)$$

which must satisfy the reproducibility requirement such that:

$$\mathbb{E}_{Y|X}[\psi(Y)|X = \mathbf{x}] = \langle h, \mu_{Y|X} \rangle_{\mathcal{F}} \quad \forall h \in \mathcal{F}, \quad (4)$$

where  $\phi(\mathbf{x}) : \Omega_X \rightarrow \mathcal{H}$ ,  $\psi(Y) : \Omega_Y \rightarrow \mathcal{F}$  and  $\mathcal{C}_{Y|X}$  is an operator  $\mathcal{H} \rightarrow \mathcal{F}$ .

Unlike the case of a marginal distribution, the embedding of a conditional distribution does not result in a single element in the RKHS but rather a family of points, each indexed by a fixed value  $\mathbf{x}$  of the conditioning variable  $X$ , thus, to obtain a single RKHS element

$\mu_{Y|X} \in \mathcal{F}$ , we need to fix  $X$  to a particular value  $\mathbf{x}$ . Therefore, the operator  $\mathcal{C}_{Y|X}$  takes as input a given  $\mathbf{x}$  and outputs an embedding. Based on Song et al. [34], the operator  $\mathcal{C}_{Y|X}$  is defined as

$$\mathcal{C}_{Y|X} = \mathcal{C}_{YX} \mathcal{C}_{XX}^{-1} = \mathbb{E}_{YX} [\psi(Y) \otimes \phi(X)] \mathbb{E}_{XX}^{-1} [\psi(X) \otimes \phi(X)], \quad (5)$$

where  $N$  is the number of samples,  $\mathcal{C}_{YX}$  and  $\mathcal{C}_{XX}$  are the cross-covariance and self-covariance operators, respectively. Given an available dataset  $\mathcal{D} = \{(\mathbf{x}_i, \mathbf{y}_i)\}_{i=1}^N$ , the empirical estimator of the operator  $\mathcal{C}_{Y|X}$  can be computed as

$$\hat{\mathcal{C}}_{Y|X} = \hat{\mathcal{C}}_{YX} \hat{\mathcal{C}}_{XX}^{-1} = \Phi(\mathbf{K} + \lambda N \mathbf{I})^{-1} \Upsilon^\top, \quad (6)$$

where  $\Phi := (\psi(\mathbf{y}_1), \dots, \psi(\mathbf{y}_N))$ ,  $\Upsilon := (\phi(\mathbf{x}_1), \dots, \phi(\mathbf{x}_N))$  and  $\mathbf{K} = \Upsilon^\top \Upsilon$  is the Gram matrix for the samples generated from  $X$ . To avoid overfitting, an additional regularization parameter  $\lambda$  is added.

### 3.2.2. Conditional embedding operator discrepancy (CEOD)

Given two datasets  $\mathcal{D}_p = \{(\mathbf{x}_i, \mathbf{y}_i)\}_{i=1}^{N_1}$  and  $\mathcal{D}_q = \{(\mathbf{x}_i, \mathbf{y}_i)\}_{i=1}^{N_2}$ , MMD measures the discrepancy between the mean embeddings using a Hilbert-Schmidt norm as  $D_{\text{MMD}}(\mathcal{D}_p, \mathcal{D}_q) = \|\hat{\mu}_{X_p} - \hat{\mu}_{X_q}\|_{HS}^2$ . Inspired by the MMD, Liu et al. [20], recently proposed the Conditional Embedding Operator Discrepancy (CEOD) for measuring the divergence between conditional distributions. The COED is based on empirical conditional embedding operators and is constructed as

$$\begin{aligned} D_{\text{CEOD}}(\mathcal{D}_p, \mathcal{D}_q) &= \left\| \hat{\mathcal{C}}_{Y_p|X_p} - \hat{\mathcal{C}}_{Y_q|X_q} \right\|_{HS}^2 \\ &= \left\| \Phi(Y_p)(\mathbf{K}_{X_p X_p} + \lambda N_1 \mathbf{I})^{-1} \Upsilon^\top(X_p) \right. \\ &\quad \left. - \Phi(Y_q)(\mathbf{K}_{X_q X_q} + \lambda N_2 \mathbf{I})^{-1} \Upsilon^\top(X_q) \right\|_{HS}^2 \\ &= \text{Tr} \left\{ (\mathbf{K}_{X_p X_p} + \lambda N_1 \mathbf{I})^{-1} \mathbf{K}_{Y_p Y_p} (\mathbf{K}_{X_p X_p} + \lambda N_1 \mathbf{I})^{-1} \mathbf{K}_{X_p X_p} \right\} \\ &\quad + \text{Tr} \left\{ (\mathbf{K}_{X_q X_q} + \lambda N_2 \mathbf{I})^{-1} \mathbf{K}_{Y_q Y_q} (\mathbf{K}_{X_q X_q} + \lambda N_2 \mathbf{I})^{-1} \mathbf{K}_{X_q X_q} \right\} \\ &\quad - 2 \text{Tr} \left\{ (\mathbf{K}_{X_p X_p} + \lambda N_1 \mathbf{I})^{-1} \mathbf{K}_{Y_p Y_q} (\mathbf{K}_{X_q X_q} + \lambda N_2 \mathbf{I})^{-1} \mathbf{K}_{X_q X_p} \right\}, \end{aligned} \quad (7)$$

where  $\mathbf{K}_{XX'}(i, j) = k(\mathbf{x}_i, \mathbf{x}'_j)$  is the Gram matrix calculated with a Gaussian kernel  $k$ .

We note that methods relied on kernel embeddings may be expensive. For this reason, a low-rank approximation of the Gram matrix, such as incomplete Cholesky factorization can be used, which allows for the reduction of computational cost while maintaining sufficient precision [33]. In this work, the CEOD will be used as part of the hybrid loss used to train the target surrogate model after the transferring of trained variables from the source surrogate as elucidated in the sequel.

### 3.3. Steps of the proposed method

#### 3.3.1. Source DeepONet training

A source DeepONet surrogate ( $\mathbf{S}$ ) is trained in a source domain  $\mathcal{D}_s = \{(\mathbf{x}_i^s, \mathbf{y}_i^s)\}_{i=1}^{N_s}$ , where  $\mathbf{x}_i^s \in \mathcal{X}_s$  and  $\mathbf{y}_i^s \in \mathcal{Y}_s$ . Any neural network architecture can be chosen for the branch net and the trunk net of the DeepONet to encode the input function and spatio-temporal coordinates

respectively. The source model is trained with a standard regression loss  $\mathcal{L}_r(\theta^S)$ , such as the relative  $L_2$  error

$$\mathcal{L}(\theta^S) = \mathcal{L}_r(\theta^S) = \frac{\|f_S(\mathbf{x}^s) - \mathbf{y}^s\|_2}{\|\mathbf{y}^s\|_2}, \quad (8)$$

where  $\|\cdot\|_2$  denotes the standard Euclidean norm and  $f_S(\mathbf{x}^s), \mathbf{y}^s$  are the prediction and reference responses respectively. Alternative error measures such as the mean-square error (MSE) can also be employed. Minimizing the loss is performed using the stochastic gradient descent (SGD) algorithm. After training the solution operator  $\mathcal{G}_{\theta^S}$  is learned and the trained parameters of the network  $\theta^{S*}$  are saved. In Figure 1, a schematic of the overall approach is presented, where the source training is depicted inside the blue box.

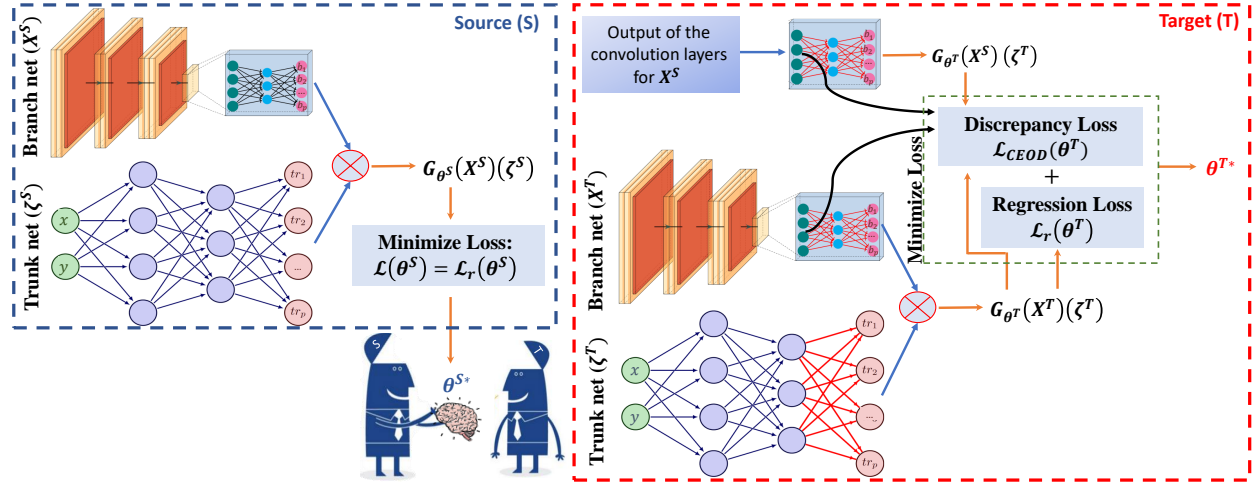


Figure 1: The proposed transfer learning framework to approximate PDE dynamics using the standard DeepONet. The source model, **(S)** (blue box), aims to learn the mapping from  $\mathbf{X}$  (input to the branch net) to the solution, employing a solution operator,  $\mathcal{G}_{\theta^S}$ , evaluated at  $\zeta^S$  locations, where  $\theta^S$  denotes the trainable parameters of the source DeepONet. The loss function,  $\mathcal{L}(\theta^S)$ , obtained as the residual loss,  $\mathcal{L}_r(\theta^S)$ , is minimized to obtain the optimized parameters of the network,  $\theta^{S*}$ . The optimized trainable parameters of the source model are transferred to the target model. All the layers of the target model (red box) are frozen except for the last layer of the trunk net and the fully-connected layers of the convolutional neural network in the branch net (shown with red arrows). Parameters associated with these layers are fine-tuned based on a hybrid loss function  $\mathcal{L}(\theta^T)$ , which is minimized to obtain the optimized parameters of the target model,  $\theta^{T*}$ .

### 3.3.2. Parameters transfer

The trained parameters of the source DeepONet **S**, are transferred to the target DeepONet **T**, for better initialization. As discussed previously, domain-invariant features transferred to the target model provide better initialization of the network which alleviates the computational cost of training from scratch with random initialization. Furthermore, this approach addresses the issue of overfitting when very few target samples are available. In addition, the architecture of the network **T** (both the branch and the trunk network) remains identical. Certain layers of **T** are freezed while others are finetuned as described next. In Figure 1, the training of target DeepONet, after the transferring of the trained source parameters  $\theta^{S*}$ , is presented (red box).

### 3.3.3. Target DeepONet finetune

As discussed previously, training the DeepONet surrogate with scarce target data can lead to overfitting. Hence, certain task-specific layers of the network are finetuned while others remain freezed with constant parameters. Commonly in computer vision, it is widely accepted that the convolutional layers are general, while fully-connected layers are task-specific [20, 35]. Adapting this concept in DNNs, we propose the fine-tuning of the fully-connected network of the branch CNN  $\{f_{b_1}^l, \dots, f_{b_m}^l\}$ , where  $m$  is the total number of layers, and the last layer of the trunk net  $f_t^l$ , to allow for sufficient expressivity during the training of the target DeepONet while maintaining the training cost low. In Figure 1, the task-specific layers are denoted with red arrows.

### 3.3.4. Hybrid loss function

Finally, we train the target model  $\mathbf{T}$ , based on a hybrid loss  $\mathcal{L}(\theta^T)$ , which considers not only the accurate match between individual target samples, but also the agreement between the conditional distributions of target data. The regression loss  $\mathcal{L}_r(\theta^T)$ , is simply computed as in Eq. 8, for the target domain data  $\mathcal{D}_t = \{(\mathbf{x}_i^{tL}, \mathbf{y}_i^{tL})\}_{i=1}^{N_t}$ . To compute the CEOD loss  $\mathcal{L}_{\text{CEOD}}(\theta^T)$  [20], we consider as input data the output of the first fully-connected layer of the branch net  $f_{b_1}^l$ , which we denote as  $\mathbf{x}_{b_1}$ . Then, we measure the conditional distribution discrepancy (Eq. 7) between the labeled data  $\mathcal{D}_t^L = \{(\mathbf{x}_{b_1i}^{tL}, \mathbf{y}_i^{tL})\}_{i=1}^{N_t}$  and unlabeled data  $\mathcal{D}_t^U = \{(\mathbf{x}_{b_1i}^{tU}, f_T(\mathbf{x}_i^{tU}))\}_{i=1}^{N_u}$ . Considering both components, the hybrid loss reads

$$\begin{aligned} \mathcal{L}(\theta^T) &= \lambda_1 \mathcal{L}_r(\theta^T) + \lambda_2 \mathcal{L}_{\text{CEOD}}(\theta^T) \\ &= \lambda_1 \frac{\|f_T(\mathbf{x}^{tL}) - \mathbf{y}^{tL}\|_2}{\|\mathbf{y}^{tL}\|_2} + \lambda_2 \left\| \hat{\mathcal{C}}_{Y_{tL}|X_{tL}} - \hat{\mathcal{C}}_{Y_{tU}|X_{tU}} \right\|_{HS}^2 \end{aligned} \quad (9)$$

where  $\lambda_1 = 1$  and  $\lambda_2 >> \lambda_1$  is a trainable coefficient which determine the importance of the two loss components during the optimization process. The trainable coefficients are updated during backpropagation. During fine-tuning of the target model, we simultaneously minimize the loss function,  $\mathcal{L}(\theta^T)$  with respect to  $\theta^T$ , and maximize the loss function with respect to  $\lambda_2$ . This approach progressively penalizes the target network for the discrepancy in the conditional probabilities of the two tasks. An important aspect of this approach is the initialization of  $\lambda_2$  at the inception of optimization, which is problem specific. For all the problems presented in this work, we have initialized  $\lambda_2 = 10$  at the beginning of the training. By training the surrogate  $\mathbf{T}$ , based on the hybrid loss in Eq. 9, we obtain the optimized parameters  $\theta^{T*}$ . In the next Section, we demonstrate the advantages of the proposed approach for task-specific operator learning under scarce data.

## 4. Experimental Results

In this Section, we provide a comprehensive collection of transfer learning problems for parametric PDEs to evaluate the validity of the proposed approach. A visual description of the different benchmarks considered is presented in Figure 2. We first introduce the benchmark problems along with the transfer learning scenarios considered, and then provide the experimental results.

Application	Input Function	Model Output	Domain Visualization	
			Source	Target/s
Darcy Flow	Random conductivity field $h(\mathbf{x}) \sim \mathcal{GP}(0, \mathcal{K}(\mathbf{x}, \mathbf{x}'))$ $\mathcal{K}(\mathbf{x}, \mathbf{x}') = \exp[-\frac{(\mathbf{x}-\mathbf{x}')^2}{2l^2}]$ $l = 0.25, \mathbf{x}, \mathbf{x}' \in [0, 1]^2$	$\nabla \cdot (K(\mathbf{x}) \nabla h(\mathbf{x})) = 1$ $h(\mathbf{x}) = 0 \quad \forall \mathbf{x} \in \partial\Omega$ $\mathcal{G}_\theta : K(\mathbf{x}) \rightarrow h(\mathbf{x})$		
Elasticity	Random loading conditions $f(\mathbf{x}) \sim \mathcal{GP}(0, \mathcal{K}(\mathbf{x}, \mathbf{x}'))$ $\mathcal{K}(\mathbf{x}, \mathbf{x}') = \exp[-\frac{(\mathbf{x}-\mathbf{x}')^2}{2l^2}]$ $l = 0.12, \mathbf{x}, \mathbf{x}' \in [0, 1]^2$	$\nabla \cdot \sigma + f(\mathbf{x}) = 0$ $(u, v) = 0 \quad \forall \mathbf{x} = 0$ $\mathcal{G}_\theta : f(\mathbf{x}) \rightarrow [u(\mathbf{x}), v(\mathbf{x})]$ $u(\mathbf{x}) : \text{X-Displacement}$ $v(\mathbf{x}) : \text{Y-Displacement}$		
Brusselator Diffusion-Reaction System	Random initial condition $h_2(\mathbf{x}) \sim \mathcal{GP}(h_2(\mathbf{x}) \mu(\mathbf{x}), \mathcal{K}(\mathbf{x}, \mathbf{x}'))$ $v(x, y, t=0) = h_2(x, y) \geq 0$ $\mathcal{K}(\mathbf{x}, \mathbf{x}') = \sigma^2 \exp[-\frac{(\mathbf{x}-\mathbf{x}')^2}{2l^2}]$ $l_x = 0.3, l_y = 0.4, \sigma^2 = 0.15$	$\frac{\partial u}{\partial t} = D_0 \nabla^2 u + a - (1-b)u + vu^2$ $\frac{\partial v}{\partial t} = D_0 \nabla^2 v + bu - vu^2$ $\mathbf{x} \in [0, 1]^2 \quad t \in [0, 1]$ $\mathcal{G}_\theta : h_2(x, y) \rightarrow v(x, y, t)$		

Figure 2: A schematic representation of the operator learning benchmarks under consideration in this work. The input/output functions and representative plots of the source and the target domains are shown.

#### 4.1. Darcy flow

Darcy's law describes the pressure of a fluid flowing through a porous medium with a given permeability and can be mathematically expressed by the following system of equations:

$$\nabla \cdot (K(\mathbf{x}) \nabla h(\mathbf{x})) = g(\mathbf{x}), \quad \mathbf{x} = (x, y), \quad (10)$$

subject to the following boundary conditions

$$h(\mathbf{x}) = 0, \quad \forall \mathbf{x} \in \partial\Omega,$$

where  $K(\mathbf{x})$  is the spatially varying hydraulic conductivity of the heterogeneous porous media, and  $h(\mathbf{x})$  is the corresponding hydraulic head. For simplicity, we consider a fixed forcing term, i.e.  $g(\mathbf{x}) = 1$ . Our goal is to learn the operator of the system in Eq. 10, which maps the input random conductivity field to the output hydraulic head, i.e.,  $\mathcal{G}_\theta : K(\mathbf{x}) \rightarrow h(\mathbf{x})$ . To generate multiple permeability fields to train the DeepONet, we describe the conductivity field  $K(\mathbf{x})$ , as a stochastic process. The source simulation box is a square domain  $\Omega = [0, 1] \times [0, 1]$ , discretized with  $d = 1541$  mesh points. We consider the following three transfer learning scenarios, which are also visually presented in Figure 2:

- **TL1:** Transfer learning from a square domain (**S**) to an equilateral triangle (**T**).
- **TL2:** Transfer learning from a square domain (**S**) to a right-angled triangle (**T**).

- **TL3:** Transfer learning from a square domain with one vertical notch (**S**) to a square domain with two horizontal notches (**T**).

Table 1: Relative  $L_2$  error and training cost in seconds ( $s$ ) for all Darcy flow problems (TL1 - TL3).

	# of training data ( $N_t$ )	TL1		TL2		TL3	
		$L_2$ (%)	time (s)	$L_2$ (%)	time (s)	$L_2$ (%)	time (s)
Training <b>S</b>	2,000	0.9	15,260	0.9	15,260	1.6	2,261
Training <b>T</b> from scratch	2,000	1.6	12,880	1.3	18,200	1.8	3,978
	5	14.2	11	9.7	10	9.6	83
	20	10.5	129	8.88	116	7.0	139
Training <b>T</b> w/ transfer learning	50	8.89	416	7.0	399	6.9	289
	100	7.11	439	5.3	437	5.0	300
	150	5.4	459	4.5	439	3.7	302
	200	4.3	462	4.2	480	3.2	304
	250	3.7	531	4.0	528	2.8	305

To train the source DeepONet, **S**, we generate  $N_s = 2,000$  source data and test on an additional set of  $N_{\text{test}}^s = 200$  samples. We consider that only a few target data are available thus generate  $N_t = 250$  target data and  $N_{\text{test}}^t = 50$  additional test data. For all PDE benchmarks, the target DeepONet, **T**, is trained for  $N_t = \{5, 20, 50, 100, 150, 200, 250\}$  samples to evaluate the effect of target dataset size. For all applications, we employ a CNN for the branch net and a FNN for the trunk net of the DeepONet. We train the DeepONet models on a single NVIDIA RTX A6000 GPU until convergence of the loss function and provide the wall clock time in seconds.

The experimental results for all three task-specific training for the Darcy system are presented in Table 1. Training the target DeepONet **T** from scratch, with random initialization and  $N_t = 2,000$  training samples results in a 1.6%, 1.3% and 1.8% error for the three TL tasks, respectively and a high computational cost. The utilization of the learned source operator by transferring the trained parameters to the target model leads to a very good accuracy even with when scarce data are available. We observe that for  $N_t = 200$  samples, transfer learning allows us to achieve small errors ( $L_2 < 5\%$ ) while keeping the computational cost very low. More specifically, the transfer learning results in 29 $\times$ , 38 $\times$  and 13 $\times$  faster training (and convergence) for TL1, TL2, and TL3 tasks, respectively, compared to the cost of training from scratch with random initialization and a large training data set. As expected the optimal accuracy achieved via transfer learning under scarce data is lower than the accuracy of training from scratch, however we observe that this discrepancy is rather small. Finally, we show representative results for each task-specific learning in Figure 3.

#### 4.2. Elasticity model

In this example, we consider a thin rectangular plate subjected to in-plane loading that is modeled as a two-dimensional problem of plane stress elasticity. The relevant equations are given below.

$$\nabla \cdot \sigma + f(\mathbf{x}), \quad \mathbf{x} = (x, y), \quad (11)$$

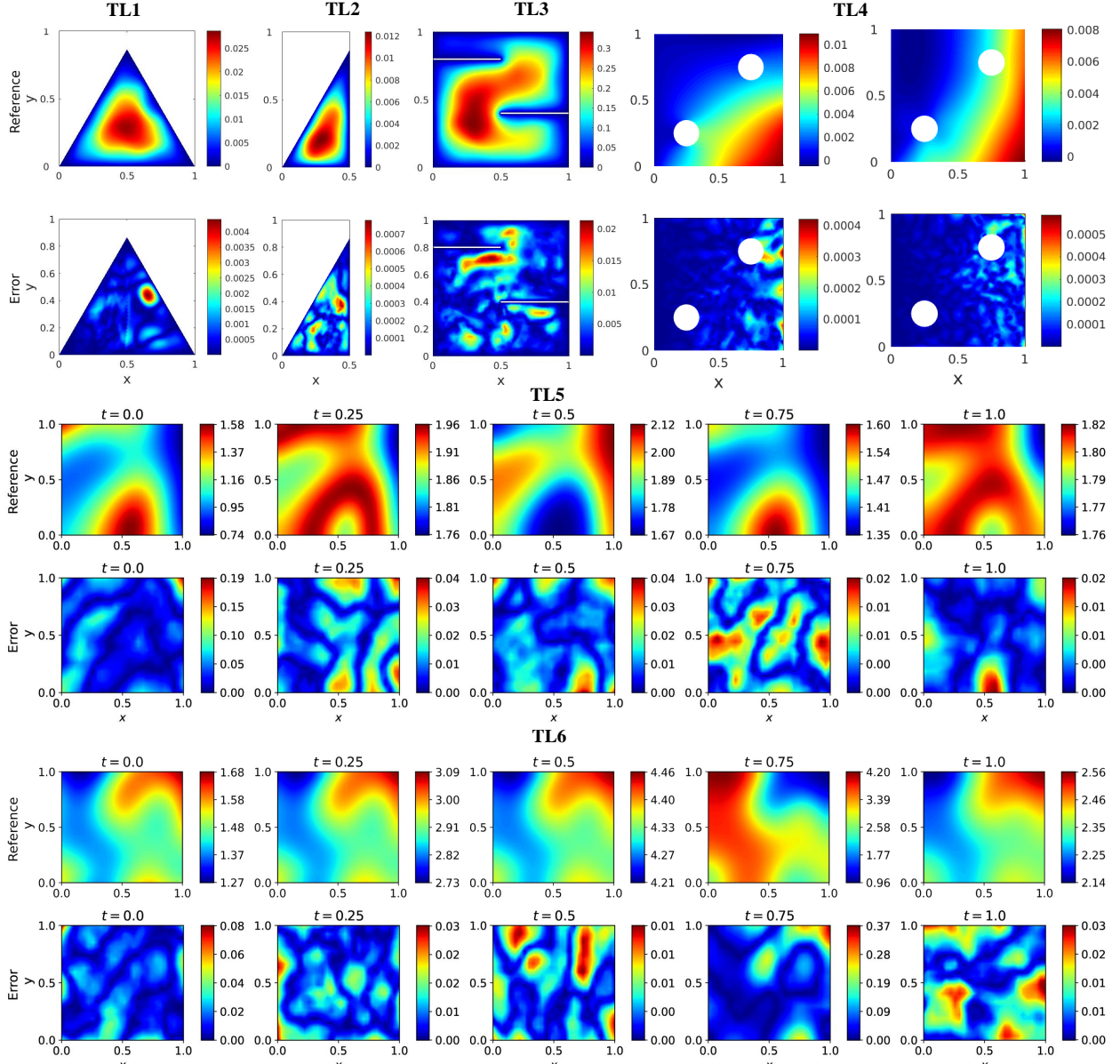


Figure 3: Representative results for all transfer learning problems: the Darcy model (TL1-TL3) takes as input the spatially varying conductivity field and approximates the hydraulic head over the domain, the elasticity model (TL4) takes as input the loading condition applied on the right edge of the plate, and outputs the displacement field. Finally, TL5, and TL6 are the approximations of the Brusselator reaction-diffusion system, which takes as input the initial random field depicting the concentration of one of the species. TL5 approximates the transfer of knowledge from a system with damped oscillations to overdamped oscillations, while TL6 represents the transfer to a system with periodic oscillations.

$$(\mathbf{u}, \mathbf{v}) = 0, \quad \forall x = 0$$

where  $u(\mathbf{x})$  and  $v(\mathbf{x})$  represent the  $x$ - and  $y$ -displacement, respectively. In addition,  $E, \nu$  represent the Young's modulus and Poisson's ratio of the material, respectively. For the source model  $\mathbf{S}$ , we consider a plate with a circular hole in the center of the simulation box

subjected to uniaxial tension. The presence of a circular hole in the plate, in the source domain, disrupts the uniform stress distribution near the hole, resulting in significantly higher than average stress.

Table 2: Relative  $L_2$  error and training cost in seconds ( $s$ ) for the elasticity transfer learning problem (TL4).

	# of training data ( $N_t$ )	$L_2$ (%)		
		$u(\mathbf{x})$	$v(\mathbf{x})$	time (s)
Training $\mathbf{S}$	1,900	2.2	2.4	10884
Training $\mathbf{T}$ from scratch	1,900	1.7	2.6	10780
	5	8.19	12.27	53
	20	5.7	10.9	148
Training $\mathbf{T}$ w/ transfer learning	50	4.4	9.8	264
	100	4.13	6.6	376
	150	3.9	5.9	418
	200	3.5	4.7	509
	250	3.33	4.62	515

We model the loading conditions  $f(\mathbf{x})$  applied to the right edge of the plate, as a Gaussian random field (see Figure 2), and we aim to learn the mapping from the random boundary load, to the displacement field ( $\mathbf{u}$ :  $x$ -displacement and  $\mathbf{v}$ :  $y$ -displacement), such that  $\mathcal{G}_\theta : f(\mathbf{x}) \rightarrow [\mathbf{u}(\mathbf{x}), \mathbf{v}(\mathbf{x})]$ . Therefore, we train the DeepONet surrogate to predict two distinct model outputs. In this example, we consider the following TL scenario:

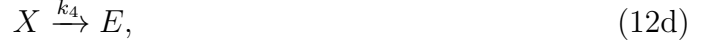
- **TL4:** Transfer learning from displacement fields with a centered hole and material properties ( $E_S, \nu_S$ ) to displacement fields with two smaller holes in the upper right and lower left corners and different material properties ( $E_T, \nu_T$ ).

The plate used in the source model has properties simulated with  $E_S = 300 \times 10^5$ , and  $\nu_S = 0.3$ , while the target model plate is simulated using  $E_T = 410 \times 10^3$ , and  $\nu_T = 0.35$ . To train the source DeepONet  $\mathbf{S}$ , we generate  $N_s = 1,900$  source data and test on an additional set of  $N_{\text{test}}^s = 100$  samples. Furthermore, we generate  $N_t = 250$  target data and  $N_{\text{test}}^t = 50$  additional test data. Detailed results are shown in Table 2. Transfer learning allows accurate predictions of the displacement fields  $u, v$  for as few as 50 and 200 target samples, respectively. Significant computational savings are achieved, as transfer learning allows  $21 \times$  acceleration of the training process compared to random initialization. A representative result for a given input realization is shown in Figure 3. We observe that the proposed TL approach allows for task-specific learning even in cases where the source and target domains are characterized by different geometry and different material properties.

#### 4.3. Brusselator diffusion-reaction system

Finally, we consider the Brusselator diffusion-reaction system, which describes an auto-catalytic chemical reaction in which a reactant substance interacts with another substance

to increase its production rate [36]. The Brusselator system is characterized by the following reactions.



where  $k_i$ , ( $i = 1, 2, 3, 4$ ) are positive parameters representing the reaction rate constant. In Eq. (12), a reactant,  $A$  is converted to a final product  $E$ , in four steps with the help of four additional species,  $X, B, Y$ , and  $D$ . Species  $A$  and  $B$  are in vast excess and thus can be modeled at constant concentration. The two-dimensional rate equations read:

$$\begin{aligned} \frac{\partial u}{\partial t} &= D_0 \left( \frac{\partial^2 u}{\partial x^2} + \frac{\partial^2 u}{\partial y^2} \right) + a - (1+b)u + vu^2, \\ \frac{\partial v}{\partial t} &= D_1 \left( \frac{\partial^2 v}{\partial x^2} + \frac{\partial^2 v}{\partial y^2} \right) + bu - vu^2, \quad \mathbf{x} \in [0, 1]^2, \quad t \in [0, 1], \end{aligned} \quad (13)$$

subject to the following initial conditions:

$$\begin{aligned} u(\mathbf{x}, t=0) &= h_1(\mathbf{x}) \geq 0, \\ v(\mathbf{x}, t=0) &= h_2(\mathbf{x}) \geq 0, \end{aligned}$$

where  $\mathbf{x} = (x, y)$  are the spatial coordinates,  $D_0, D_1$  represent the diffusion coefficients,  $a = \{A\}, b = \{B\}$  are constant concentrations, and  $u = \{X\}, v = \{Y\}$  represent the concentrations of reactant species  $X, Y$ . We train DeepONet surrogates to learn the mapping between the initial field and the evolved concentration of species  $v$ , i.e.  $\mathcal{G}_\theta : h_2(\mathbf{x}) \rightarrow v(\mathbf{x}, t)$ . The initial field  $h_2(x, y)$  is modeled as a Gaussian random field. The following two transfer learning problems are considered (see Figure 2):

- **TL5:** Transfer learning from damped oscillations to overdamped oscillations (approaching fast a steady-state response).
- **TL6:** Transfer learning from damped oscillations to periodic oscillations (limit cycle in phase space).

The Brusselator dynamics can be controlled by the constant concentration  $b = \{B\}$  which we set as  $b_S = 2.2$  and  $b_{T_1} = 1.7, b_{T_2} = 3.0$  for the source and two target tasks respectively. We generate  $N_s = 800$  for the source DeepONet  $\mathbf{S}$ , source data, and  $N_{\text{test}}^s = 200$  test samples. In addition, we generate  $N_t = 250$ ,  $N_{\text{test}}^t = 50$  train and test target data for training the target model  $\mathbf{T}$ . The results for both TL5 and TL6 problems are presented in Table 3. For the case where the TL task involves the learning of the overdamped oscillations (TL5), we observe that the target DeepONet  $\mathbf{T}$ , achieves very high accuracy for  $N_t > 50$  samples. Interestingly, as we increase the number of target training samples, the relative  $L_2$  error converges to the result with random initialization and a plethora of available data (see Table 3, second row) while an acceleration of  $11 \times$  faster training is achieved. In contrast, for the more challenging task (TL6), where target DeepONet  $\mathbf{T}$  learns the oscillatory response, more available data are needed for accurate operator regression. However, the computational

Table 3: Relative  $L_2$  error and training cost in seconds ( $s$ ) for Brusselator transfer learning problems (TL5 & TL6).

# of training data ( $N_t$ )	TL5		TL6	
	$L_2$ (%)	time (s)	$L_2$ (%)	time (s)
Training <b>S</b>	800	1.55	3,532	1.55
Training <b>T</b> from scratch	800	1.10	2,461	2.92
	5	24.2	57	52.9
	20	15.6	132	15.7
Training <b>T</b> w/ transfer learning	50	2.40	188	12.5
	100	2.3	206	9.4
	150	2.1	209	5.9
	200	2.0	213	4.97
	250	1.99	229	4.95
				345

savings are significant, with an acceleration  $15\times$  of the training process. A representative results for both TL scenarios is presented in Figure 3, where the reference and point-wise error fields are shown for five distinct time steps.

## 5. Summary

Operator regression approaches have been successful in learning nonlinear operators for complex PDEs directly from observations. However, in many real-world applications, collecting the needed training data and rebuilding the models is either prohibitively expensive or impossible. In this study, we introduce a novel formulation to transfer the knowledge of a solution operator trained on a system of PDEs for a specific domain to a different domain. Such situations are challenging considering the conditional probability distribution of the source and the target domains are different. We demonstrate the efficacy of the proposed DeepONet based transfer learning framework by solving six different benchmark problems (employing well-known differential equations). Our observations can be summarized as follows:

- The key ingredient of the proposed approach is the formulation of the hybrid loss function (in [Equation 9](#)) that aims to reduce the discrepancy of both: individual samples and conditional distribution of the target data. As a thumb rule of this framework, the loss term involving the difference in the conditional probability of the two domains must be penalized over the regression loss. For easy maneuvering of the appropriate penalizing parameters, we have adopted these parameters to be trainable and self-adaptive during the fine tuning of the target model.
- Tasks TL1 and TL2 exhibit the ability of the approach to transfer the knowledge from a square domain to triangular domains with a computational gain of approximately  $24\times$  and  $34\times$  ([Table 1](#) columns 3-6), while maintaining an acceptable level of accuracy and operating on a data regime that is  $1/8$  of the data required for training the model

from scratch. Additionally, to test the performance of the approach on challenging situations, we consider domains with discontinuity and notches (task TL3). We observe an accuracy loss of just 1%, we can predict the hydraulic head with much smaller labelled data (250), and the solution converges  $13\times$  faster (Table 1 columns 7 and 8).

- The proposed TL framework allows for multitask learning even when source and target domains differ in more than one aspect. As demonstrated in the elasticity model (TL4), the two domains are characterized by different geometry (source domain: plate with a hole, target domain: plate with two holes) and vastly different material properties ( $E_S = 300 \times 10^5$  and  $\nu_S = 0.3$  while  $E_T = 410 \times 10^3$  and  $\nu_S = 0.35$ ). A study on the target dataset size shows that approximately 200 samples are sufficient to model the conditional shift from the source to the target domain (Table 2).
- Finally, we test our approach on a dynamical system employing a 2D time-dependent PDE for a Brusselator reaction-diffusion system. In TL6 we deploy the source model trained on smooth dynamics to be applied for approximating highly non-smooth dynamics. Our results in Table 3, show that even for such challenging dynamics, the framework performed well. For TL6, the fine-tuning of the target domain carried out using self-adaptive weights, which was used in the regression loss of the target domain.
- Overall, we found that transferring of previously-acquired knowledge (i.e., domain-invariant features learned from lower levels of the model) and fine-tuning of higher-level layers of the network allows for efficient multitask operator learning with significant computational savings when solving PDE problems under conditional distribution mismatch.

## Data availability

Datasets were generated using the *PDE Toolbox* in MATLAB and the *py-pde* python package which can be found on <https://github.com/zwicker-group/py-pde>.

## Code availability

The code used in this study will become available on the GitHub repository <https://github.com/katiana22/TL-DeepONet> upon publication of this work.

## Acknowledgements

For KK and MDS, this material is based upon work supported by the U.S. Department of Energy, Office of Science, Office of Advanced Scientific Computing Research under Award Number DE-SC0020428. SG and GEK would like to acknowledge support by the DOE project PhILMs (Award Number DE-SC0019453) and the OSD/AFOSR MURI grant FA9550-20-1-0358.

## References

- [1] R. T. Chen, Y. Rubanova, J. Bettencourt, D. K. Duvenaud, Neural ordinary differential equations, *Advances in neural information processing systems* 31 (2018).
- [2] M. Raissi, P. Perdikaris, G. E. Karniadakis, Physics-informed neural networks: A deep learning framework for solving forward and inverse problems involving nonlinear partial differential equations, *Journal of Computational Physics* 378 (2019) 686–707.
- [3] Z. Li, N. Kovachki, K. Azizzadenesheli, B. Liu, K. Bhattacharya, A. Stuart, A. Anandkumar, Fourier neural operator for parametric partial differential equations, *arXiv preprint arXiv:2010.08895* (2020).
- [4] L. Lu, P. Jin, G. Pang, Z. Zhang, G. E. Karniadakis, Learning nonlinear operators via deepenet based on the universal approximation theorem of operators, *Nature Machine Intelligence* 3 (3) (2021) 218–229.
- [5] P. C. Di Leoni, L. Lu, C. Meneveau, G. Karniadakis, T. A. Zaki, Deepenet prediction of linear instability waves in high-speed boundary layers, *arXiv preprint arXiv:2105.08697* (2021).
- [6] A. Olivier, M. D. Shields, L. Graham-Brady, Bayesian neural networks for uncertainty quantification in data-driven materials modeling, *Computer Methods in Applied Mechanics and Engineering* 386 (2021) 114079.
- [7] S. Niu, Y. Liu, J. Wang, H. Song, A decade survey of transfer learning (2010–2020), *IEEE Transactions on Artificial Intelligence* 1 (2) (2020) 151–166.
- [8] Y. Gao, K. M. Mosalam, Deep transfer learning for image-based structural damage recognition, *Computer-Aided Civil and Infrastructure Engineering* 33 (9) (2018) 748–768.
- [9] X. Yang, Y. Zhang, W. Lv, D. Wang, Image recognition of wind turbine blade damage based on a deep learning model with transfer learning and an ensemble learning classifier, *Renewable Energy* 163 (2021) 386–397.
- [10] S. Ruder, M. E. Peters, S. Swayamdipta, T. Wolf, Transfer learning in natural language processing, in: *Proceedings of the 2019 conference of the North American chapter of the association for computational linguistics: Tutorials*, 2019, pp. 15–18.
- [11] S. Zhang, M. Chen, J. Chen, Y.-F. Li, Y. Wu, M. Li, C. Zhu, Combining cross-modal knowledge transfer and semi-supervised learning for speech emotion recognition, *Knowledge-Based Systems* 229 (2021) 107340.
- [12] F. Zhuang, Z. Qi, K. Duan, D. Xi, Y. Zhu, H. Zhu, H. Xiong, Q. He, A comprehensive survey on transfer learning, *Proceedings of the IEEE* 109 (1) (2020) 43–76.
- [13] S. T. Certo, J. R. Busenbark, H.-s. Woo, M. Semadeni, Sample selection bias and heckman models in strategic management research, *Strategic Management Journal* 37 (13) (2016) 2639–2657.

- [14] X. Chen, S. Wang, J. Wang, M. Long, Representation subspace distance for domain adaptation regression, in: International Conference on Machine Learning, PMLR, 2021, pp. 1749–1759.
- [15] D. Pardoe, P. Stone, Boosting for regression transfer, in: ICML, 2010.
- [16] X. Wang, T.-K. Huang, J. Schneider, Active transfer learning under model shift, in: International Conference on Machine Learning, PMLR, 2014, pp. 1305–1313.
- [17] S. S. Du, J. Koushik, A. Singh, B. Póczos, Hypothesis transfer learning via transformation functions, *Advances in neural information processing systems* 30 (2017).
- [18] K. Zhang, B. Schölkopf, K. Muandet, Z. Wang, Domain adaptation under target and conditional shift, in: International Conference on Machine Learning, PMLR, 2013, pp. 819–827.
- [19] G. Chen, Y. Li, X. Liu, Transfer learning under conditional shift based on fuzzy residual, *IEEE Transactions on Cybernetics* (2020).
- [20] X. Liu, Y. Li, Q. Meng, G. Chen, Deep transfer learning for conditional shift in regression, *Knowledge-Based Systems* 227 (2021) 107216.
- [21] X. Zhang, K. Garikipati, Machine learning materials physics: Multi-resolution neural networks learn the free energy and nonlinear elastic response of evolving microstructures, *Computer Methods in Applied Mechanics and Engineering* 372 (2020) 113362.
- [22] S. Goswami, C. Anitescu, S. Chakraborty, T. Rabczuk, Transfer learning enhanced physics informed neural network for phase-field modeling of fracture, *Theoretical and Applied Fracture Mechanics* 106 (2020) 102447.
- [23] S. Desai, M. Mattheakis, H. Joy, P. Protopapas, S. Roberts, One-shot transfer learning of physics-informed neural networks, *arXiv preprint arXiv:2110.11286* (2021).
- [24] X. Chen, C. Gong, Q. Wan, L. Deng, Y. Wan, Y. Liu, B. Chen, J. Liu, Transfer learning for deep neural network-based partial differential equations solving, *Advances in Aerodynamics* 3 (1) (2021) 1–14.
- [25] M. Penwarden, S. Zhe, A. Narayan, R. M. Kirby, Physics-informed neural networks (pinns) for parameterized pdes: A metalearning approach, *arXiv preprint arXiv:2110.13361* (2021).
- [26] B. Neyshabur, H. Sedghi, C. Zhang, What is being transferred in transfer learning?, *Advances in neural information processing systems* 33 (2020) 512–523.
- [27] L. Lu, X. Meng, S. Cai, Z. Mao, S. Goswami, Z. Zhang, G. E. Karniadakis, A comprehensive and fair comparison of two neural operators (with practical extensions) based on fair data, *arXiv preprint arXiv:2111.05512* (2021).

- [28] K. Kontolati, S. Goswami, M. D. Shields, G. E. Karniadakis, On the influence of over-parameterization in manifold based surrogates and deep neural operators, arXiv preprint arXiv:2203.05071 (2022).
- [29] Y. K. Lee, B. U. Park, Estimation of kullback–leibler divergence by local likelihood, *Annals of the Institute of Statistical Mathematics* 58 (2) (2006) 327–340.
- [30] S. Yu, A. Shaker, F. Alesiani, J. C. Principe, Measuring the discrepancy between conditional distributions: Methods, properties and applications, arXiv preprint arXiv:2005.02196 (2020).
- [31] K. Muandet, K. Fukumizu, B. Sriperumbudur, B. Schölkopf, et al., Kernel mean embedding of distributions: A review and beyond, *Foundations and Trends® in Machine Learning* 10 (1-2) (2017) 1–141.
- [32] A. Gretton, K. M. Borgwardt, M. J. Rasch, B. Schölkopf, A. Smola, A kernel two-sample test, *The Journal of Machine Learning Research* 13 (1) (2012) 723–773.
- [33] L. Song, K. Fukumizu, A. Gretton, Kernel embeddings of conditional distributions: A unified kernel framework for nonparametric inference in graphical models, *IEEE Signal Processing Magazine* 30 (4) (2013) 98–111.
- [34] L. Song, J. Huang, A. Smola, K. Fukumizu, Hilbert space embeddings of conditional distributions with applications to dynamical systems, in: *Proceedings of the 26th Annual International Conference on Machine Learning*, 2009, pp. 961–968.
- [35] J. Yosinski, J. Clune, Y. Bengio, H. Lipson, How transferable are features in deep neural networks?, *Advances in neural information processing systems* 27 (2014).
- [36] N. Ahmed, M. Rafiq, M. Rehman, M. Iqbal, M. Ali, Numerical modeling of three dimensional brusselator reaction diffusion system, *AIP Advances* 9 (1) (2019) 015205.